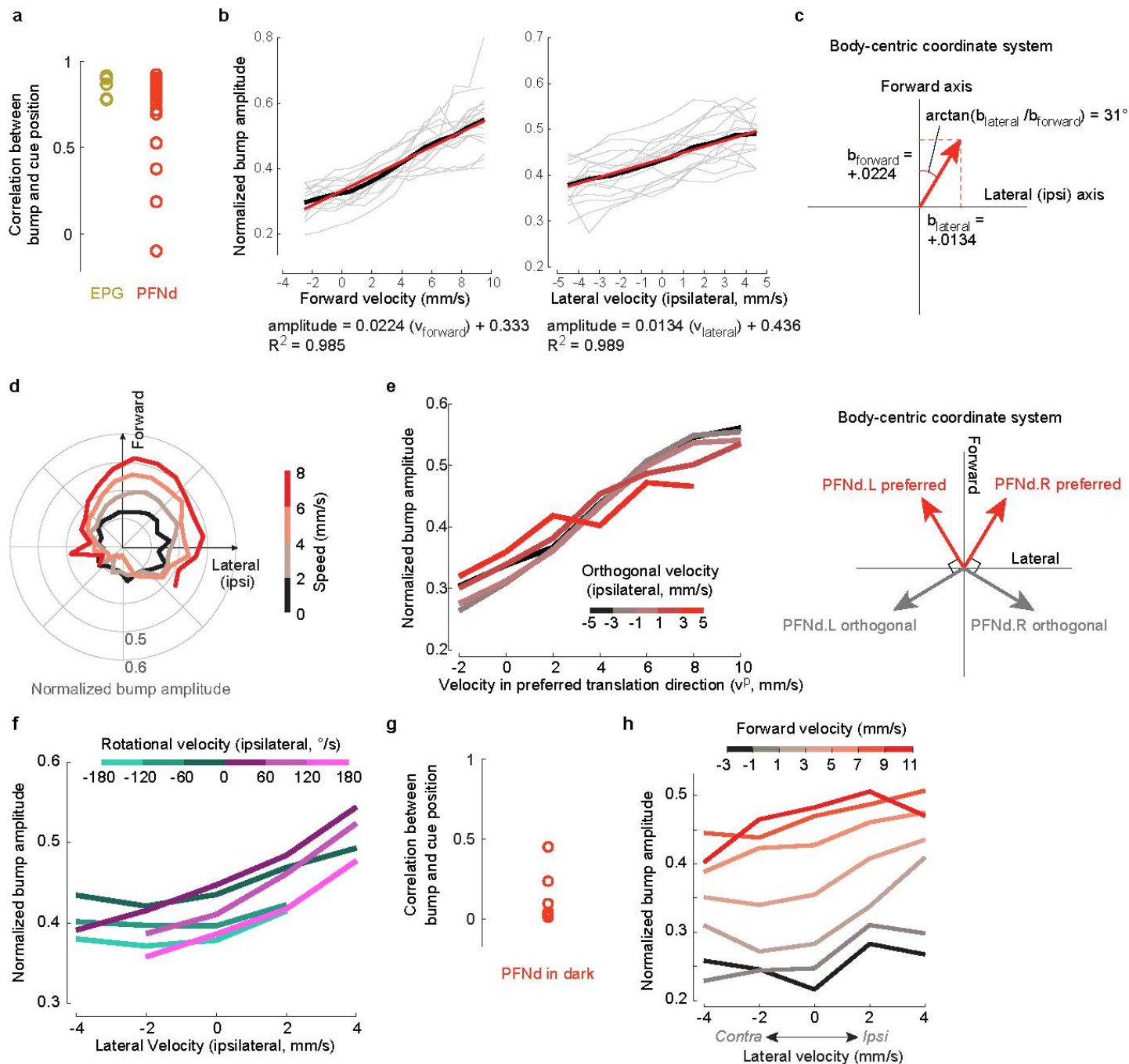


Extended Data Figure 1: Walking statistics on a spherical treadmill.

a. Distribution of forward \times lateral, forward \times rotational, and lateral \times rotational velocities. Shown along each axis is the marginal distribution (gray lines on top right of each heatmap denote scale for the marginal distribution). Data are pooled across $n=27$ flies. We used the velocities recorded at the camera sampling rate (50 Hz) prior to down-sampling to volumetric calcium imaging rate.

b. An example walking bout (30 seconds). Shown are the fly's forward, lateral, and rotational velocity as well as its heading (based on the position of the visual cue shown in closed loop; note that we used a visual closed loop gain of $0.8\times$, meaning that the landmark is displaced by an azimuthal angle equal to $0.8\times$ the ball's yaw displacement).

c. Fictive trajectory of the fly in 2D space based on the walking parameters in the example bout shown in b. The dotted line shows the calculated trajectory using only the forward velocity and the heading of the fly, ignoring the lateral velocity. The solid line shows the calculated trajectory using the forward velocity, lateral velocity, and heading of the fly. Note that the dotted line underestimates the curvature of the fly's path.



Extended Data Figure 2: PFNd tuning properties.

a. Circular correlation between bump and cue position for PFNd ($n=16$ flies) and EPG neurons ($n=5$ flies). Note that PFNd bump position is not as correlated with heading as EPG activity is. This is because PFNd neurons conjunctively encode velocity and heading, whereas EPG neurons encode only heading. For example, when the fly walks forward right, the PFNd bump on the left diminishes in amplitude, and *vice versa*. When the left and right bumps have different amplitudes, this diminishes the accuracy of our estimate of the bump position. Moreover, when the fly steps backward, both PFNd bumps diminish in amplitude, which again makes it difficult to accurately estimate bump position.

b. Normalized PFNd PB bump amplitude versus forward velocity (left), and lateral velocity (right). Gray lines are individual flies and the black line is the mean across flies ($n=16$ flies). Data from the right and left PB are combined, and lateral velocity is computed in the ipsilateral direction (so that, for PFNd.L neurons, leftward lateral velocity is positive

and rightward lateral velocity is negative). The red line shows the linear fit to the mean line, with the fitted equation below each plot.

c. Computation of preferred translational direction angle using the linear regression slopes for forward and lateral velocity. We used the ratio of the slopes of the linear fits to lateral and forward velocity to calculate the angle of preferred translational direction.

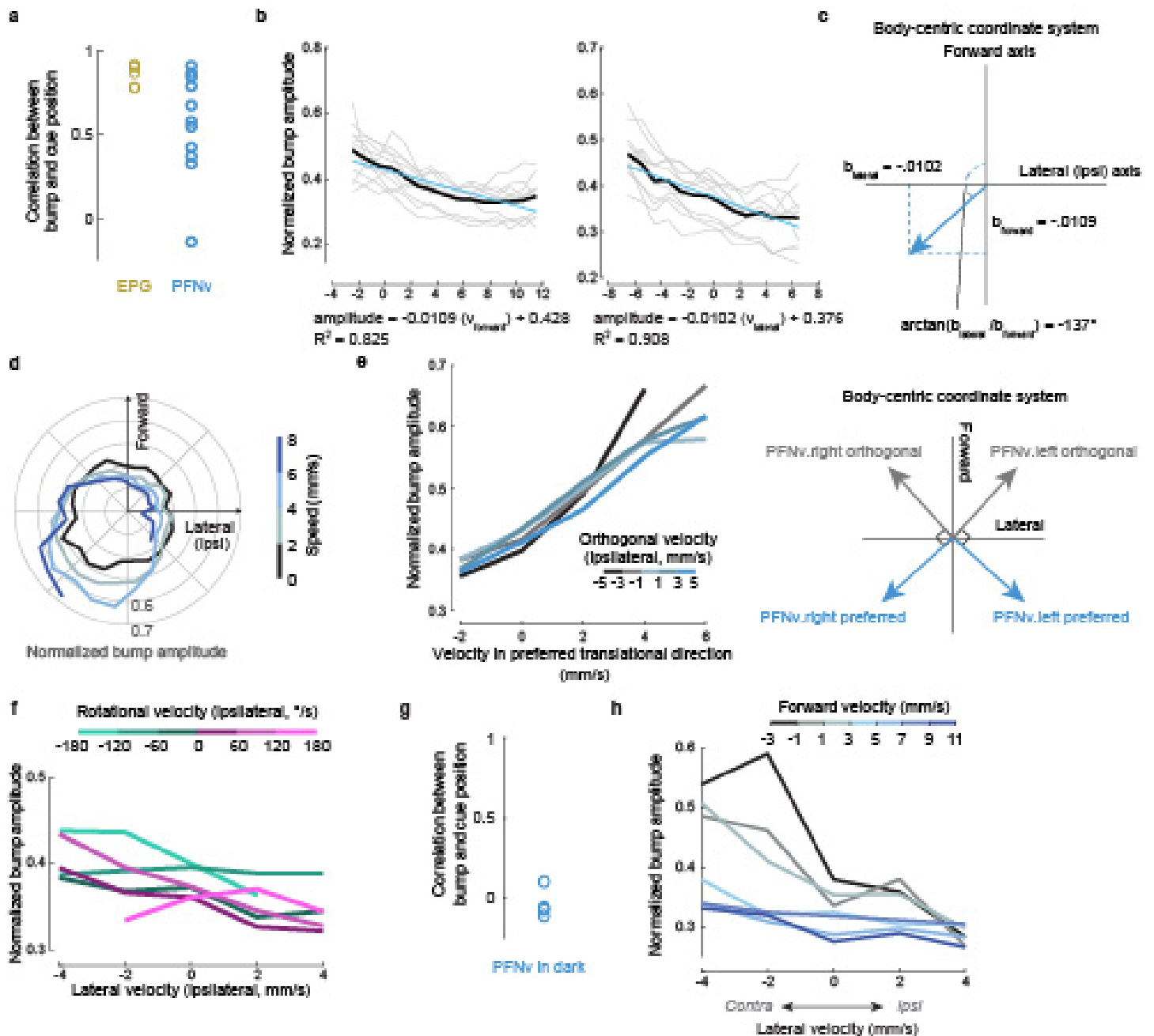
d. PFNd data from Fig. 1g, re-plotted in polar coordinates. Here, normalized bump amplitude is displayed as a function of body-centric translation direction and binned by speed.

e. Normalized PFNd bump amplitude versus velocity in the preferred translational direction (v^p). Data from the right and left PB are combined and binned by the fly's velocity orthogonal to the preferred translational direction (see schematic at right). Shown is the mean across flies (n=16 flies). Note that a positive value in the orthogonal axis is in the ipsilateral direction. Whereas there is a significant effect of velocity in the preferred direction (2-way ANCOVA, $P < 10^{-10}$), there is no significant effect of velocity in the orthogonal direction ($p=0.97$).

f. Normalized PFNd bump amplitude versus lateral velocity in the ipsilateral direction. Data from the right and left PB are combined, binned by ipsilateral rotational velocity, and averaged across flies (n=16 flies). Whereas there is a significant effect of lateral velocity (2-way ANCOVA, $P < 10^{-10}$), there is no significant effect of rotational velocity ($p=0.59$). This analysis shows that there is little or no systematic relationship between PFNd activity and rotational velocity once we account for the effect of lateral velocity. Note that, because rotational and lateral velocity are correlated, rotational velocity bins are asymmetrically populated.

g. Circular correlation between bump and cue position for PFNd neurons when the fly walks in darkness (n=7 flies).

h. Normalized bump amplitude versus lateral velocity in the ipsilateral direction, binned and color-coded by forward velocity, for PFNd neurons when the fly walks in darkness (n=7 flies). Lateral velocity is measured in the ipsilateral direction, and data from the right and left PB are combined and then averaged across flies. Both forward and lateral velocity have a significant effect (2-way ANCOVA, $P < 10^{-10}$ and $P < 10^{-5}$).



Extended Data Figure 3: PFNv tuning properties.

a. Circular correlation between bump and cue position for EPG (n=5 flies, reproduced from Extended Data Fig. 2a) and PFNv neurons (n=11 flies). Note that PFNv bump position is not as correlated with heading as EPG activity is. This is because PFNv neurons conjunctively encode velocity and heading, whereas EPG neurons encode only heading. In particular, PFNv bump amplitude is generally quite low when the fly is walking forward.

b. Normalized PFNv PB bump amplitude versus forward velocity (left), and lateral velocity (right). Gray lines correspond to individual flies and the black line corresponds to the mean across flies (n=11 flies). Data for the right and left PB are combined, and lateral velocity is computed in the ipsilateral direction. The blue line shows the linear fit to the mean line, with the fitted equation below each plot.

c. Computation of preferred translational direction angle using the linear regression slopes for forward and lateral velocity. We used the ratio of the slopes of the linear fits to lateral and forward velocity to calculate the angle of preferred translational direction.

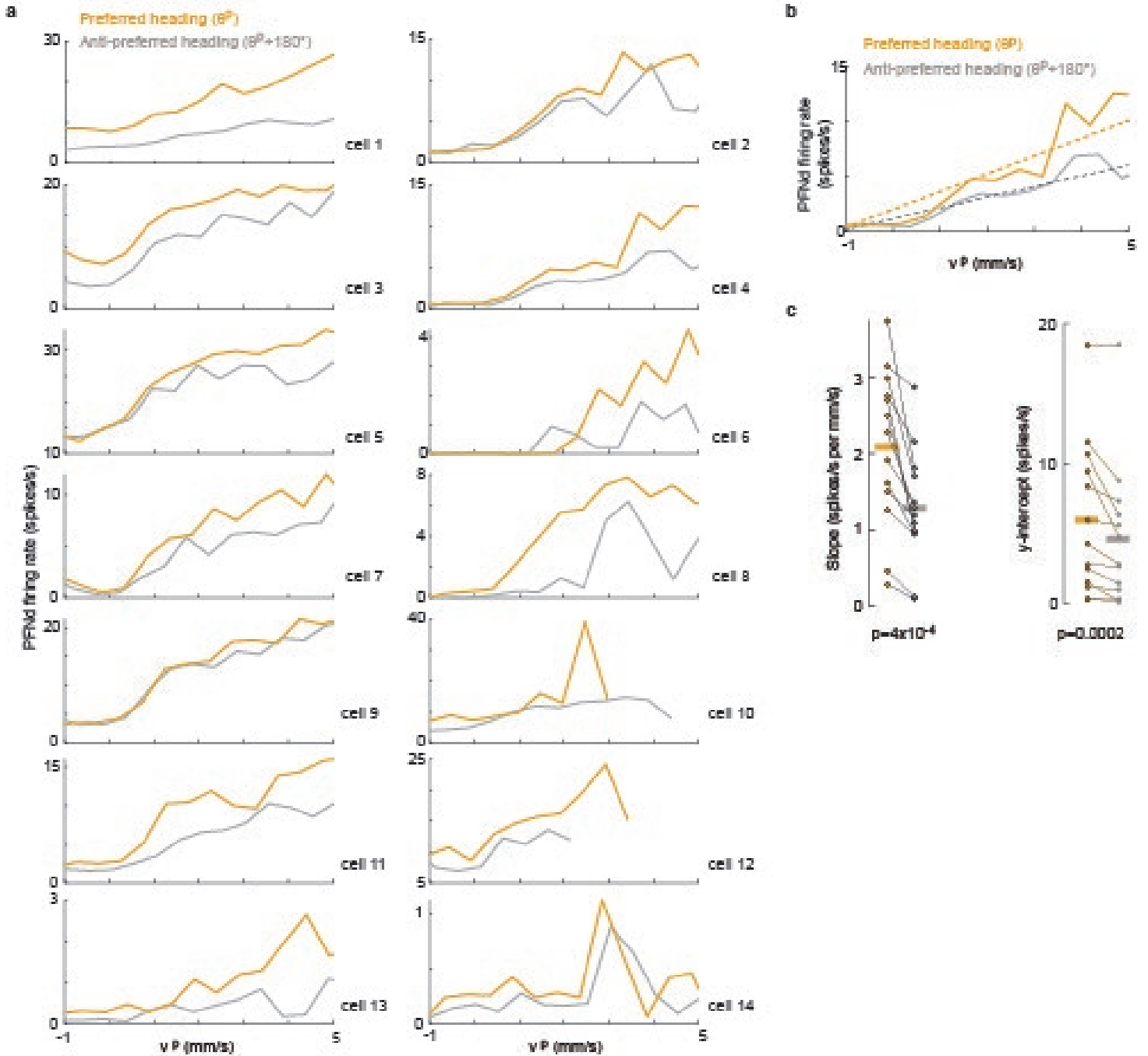
d. PFNv data from Fig. 1g, re-plotted in polar coordinates. Here, normalized bump amplitude is displayed as a function of body-centric translation direction and binned by speed.

e. Normalized PFNv bump amplitude versus velocity along the angle of preferred translational direction (v^p). Data are combined between the right and left PB and binned by the velocity along the angle of translational movement orthogonal to the preferred direction (see schematic at right). Shown is the mean across flies (n=11 flies). The orthogonal directions for the right and left PFNv population are shown (right); note that a positive value in the orthogonal axis remains in the contralateral direction for the given right/left population. Whereas there is a significant effect of velocity in the preferred direction (2-way ANCOVA, $P < 10^{-10}$), there is no significant effect of velocity in the orthogonal direction ($p=0.30$).

f. Normalized PFNv bump amplitude versus lateral velocity in the ipsilateral direction. Data for the right and left PB are combined, binned by the ipsilateral rotational velocity, and averaged across flies (n=11 flies). For this cell type, both lateral and rotational velocity have significant effects (2-way ANCOVA, $P < 10^{-10}$ and $P < 0.005$). Note that, because rotational and lateral velocity is correlated, rotational velocity bins are asymmetrically populated.

g. Circular correlation between bump and cue position for PFNv neurons when the fly walks in darkness (n=4 flies).

h. Normalized bump amplitude versus lateral velocity in the ipsilateral direction, binned and color-coded by forward velocity, for PFNv neurons when the fly walks in darkness (n=4 flies). Lateral velocity is measured in the ipsilateral direction, and data from the right and left PB are combined and then averaged across flies. Both forward and lateral velocity have a significant effect (2-way ANCOVA, $p < 10^{-7}$ for each factor).



Extended Data Figure 4: Interaction between heading and velocity tuning in PFNd neurons.

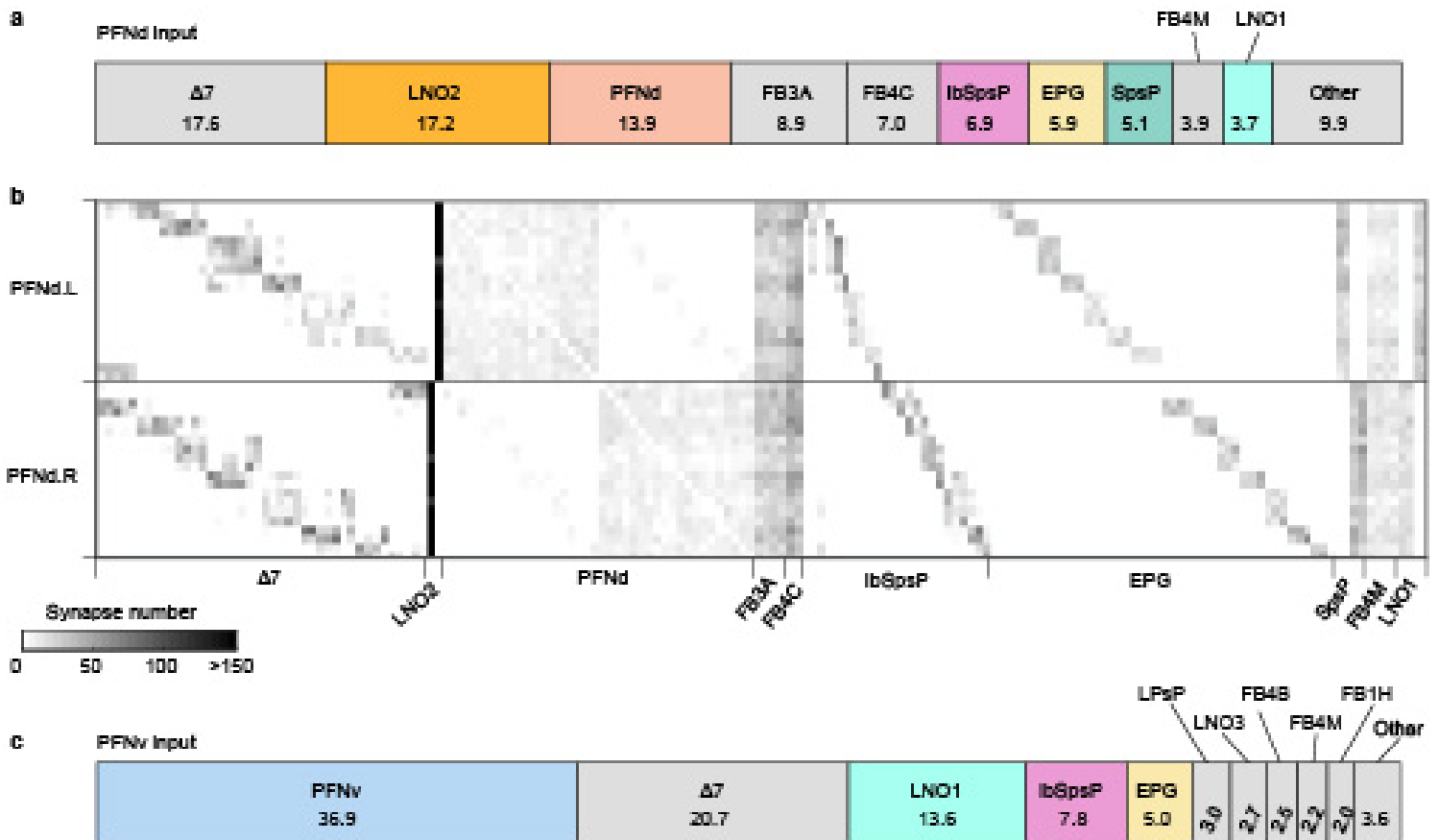
a. Firing rate versus v^p for all PFNd recordings. Data are divided into bins based on the proximity of the fly's heading to the neuron's preferred heading. Three of these cells are shown in Fig. 2b.

b. Linear fits for one example cell.

c. Fitted slope values (reproduced from Fig. 2b) and y-intercept values for all cells ($n=14$ cells in 9 flies). Horizontal lines indicate mean values. For both parameters, there is a statistically significant effect of heading (2-way paired t-tests, Bonferroni-corrected p values). However, the effect of heading on the slope is relatively large and consistent, as compared to the effect on the y-intercept, which is smaller and less consistent. This implies that the effect of heading (θ) on the cell's firing rate (f) is largely multiplicative, i.e., it controls the slope of the relationship between f and v^p , as in

$$f \propto (\cos(\theta - \theta^p) + a) v^p + b$$

where θ^p , a , and b are constants. In our computational model (Fig. 4a-d), we use this same relationship, with $\theta^p=0$, $a=1$, $b=0$.



Extended Data Figure 5: Connectomics analysis of inputs to PFNd and PFNv neurons.

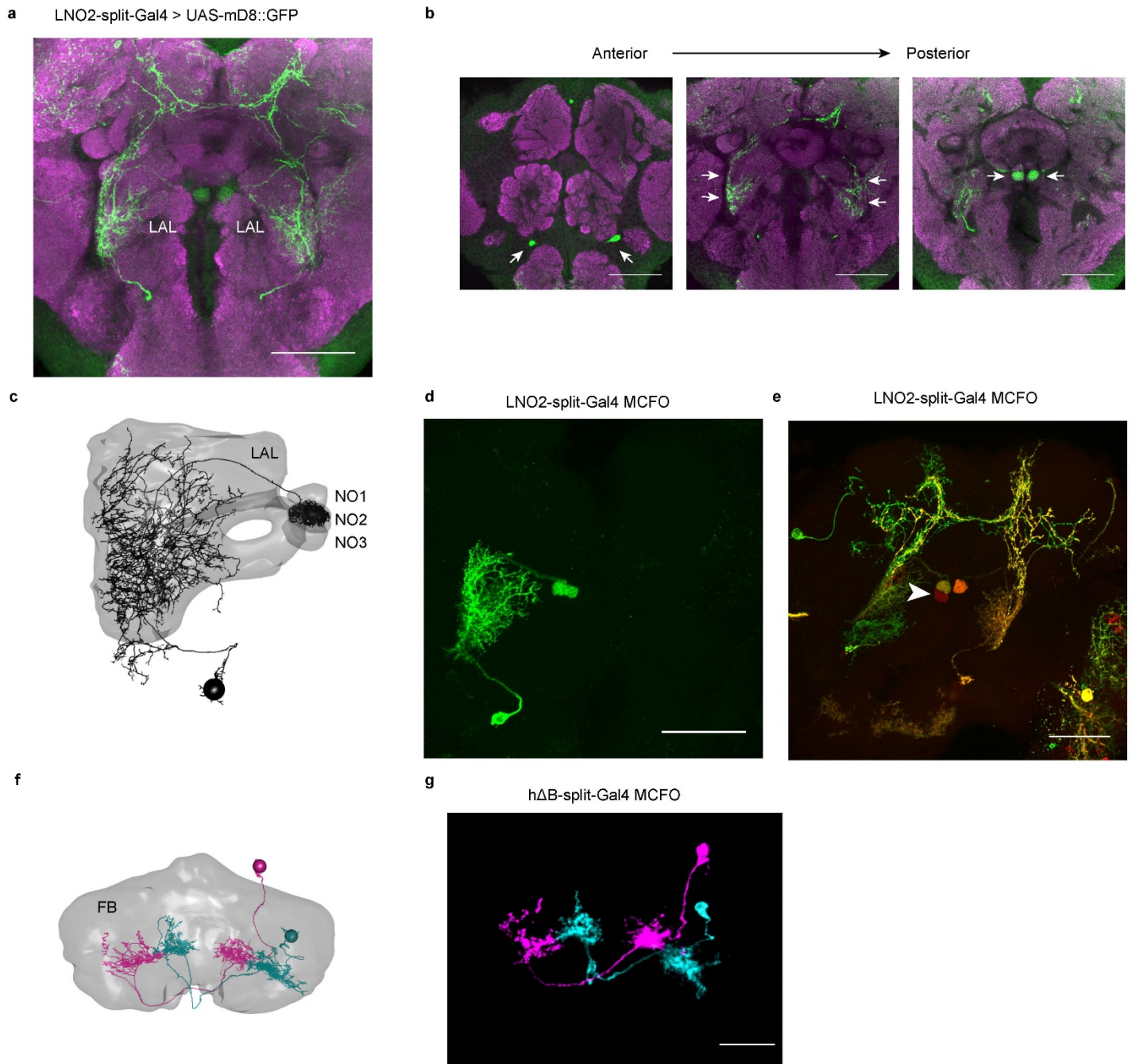
a. Distribution of input synapses onto PFNd neurons from the hemibrain connectome²⁴, grouped by cell type. Shown are the top ten cell type inputs onto PFNd neurons; all other identified cell types are grouped into “Other.” Collectively, the distribution shown comprises 94.2% of all input synapses onto PFNd neurons. Numbers indicate the percentage of synapses contributed by each input cell type. Note that $\Delta 7$ neurons and FB3A/4C/4M neurons are major inputs to PFNd neurons, but we did not screen these neurons as part of our search for the origin of body-centric velocity signals in PFNd neurons, for the following reasons:

$\Delta 7$ neurons: $\Delta 7$ population activity is known to encode the fly’s heading direction, reflecting the strong input to $\Delta 7$ neurons from EPG neurons. It has been proposed that the function of $\Delta 7$ neurons is to reshape the heading bump into a cosine-shaped activity profile^{5,34}. Thus, much of the “compass input” that we refer to in our study as originating from EPG neurons is probably due to the combined action of EPG neurons (which constitute the primary computational map of the compass system) and $\Delta 7$ neurons (which reshape and reinforce the compass system output).

FB3A/4C/4M neurons: These neurons are FB tangential cells, meaning their axons run across the entire horizontal extent of the FB, perpendicular to PFNd dendrites⁵. Like other FB tangential cells, these neurons receive input from outside the central complex and they synapse onto a variety of cell types in the FB. There is evidence that FB tangential cells encode information about context, behavioral state, and internal physiological needs, including the need for sleep⁵.

b. Input connectivity matrix for PFNd neurons, shown for the top ten input cell types. Connections comprising 3 or fewer synapses are not shown. Note that the cell types that provide major unilateral input to PFNd neurons are LNO2, IbSpsP, EPG, SpsP, and LNO1.

c. Same as (a) but for PFNv neurons. Collectively, the distribution shown comprises 93.1% of all input synapses onto PFNv neurons.



Extended Data Figure 6: LNO2 and hAB split-Gal4 line characterization.

a. GFP expression driven by the LNO2 split-Gal4 line: +; $Mi\{Trojan-p65AD.2\}VGlut[MI04979-Tp65AD.2]$; $P\{VT008681-Gal4.DBD\}attP2$. Shown is a coronal projection of a confocal stack through the anterior half of the brain. GFP staining is shown in green, and neuropil staining (nc82) is shown in magenta. The scale bar is 50 μm . Note that, in addition to targeting LNO2 neurons in the LAL, there are some cells labeled in the superior brain which are not LNO2 cells. The observation that this VGlut-split-Gal4 construct drives expression in LNO2 neurons is evidence in support of the conclusion that LNO2 neurons are glutamatergic.

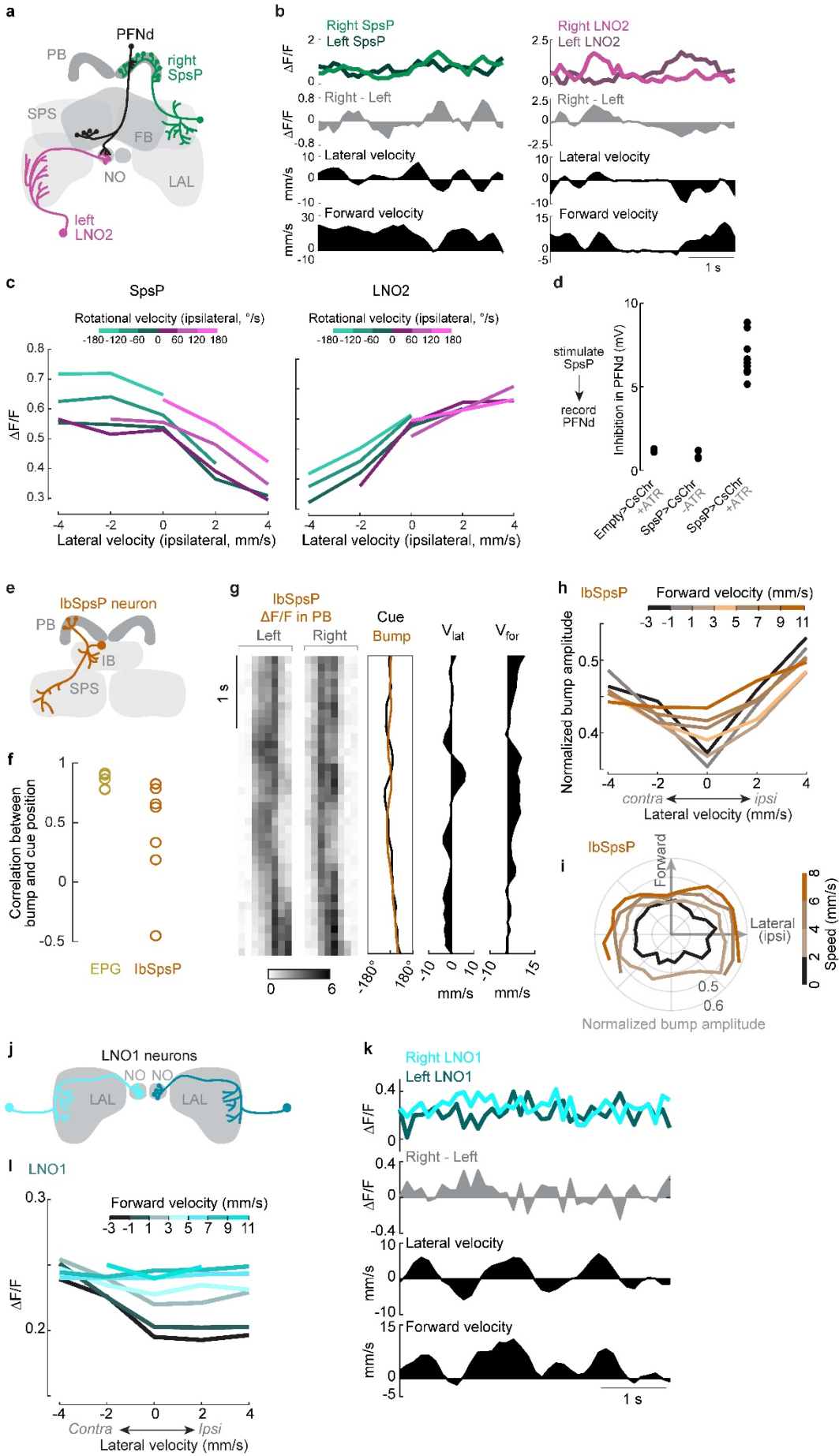
b. Same as (a) but for individual optical slices. Shown are the location of the LNO2 cell bodies (left, arrows), neurites in the LAL (middle, arrows), and neurites in NO2 (right, arrows). Scale bars are 50 μm .

c. Skeleton of LNO2 neuron from the hemibrain dataset. Overlaid are the anatomical boundaries of the LAL and the NO (divided into subunits NO1, NO2, and NO3). The black sphere denotes the position of the cell body. There is one LNO2 neuron per hemisphere.

d. MCFO labeling of a single LNO2 neuron from the LNO2-split Gal4 line. Scale bar is 50 μm .

e. On occasion, the LNO2 split-Gal4 line shows expression in NO3. Shown is an MCFO sample from the LNO2-split Gal4 line that labels this additional neuron in NO3 (arrow). Given that two channels (green and red) label the LNO2 on the ipsilateral side, whereas only one channel (red) shows the NO3-innervating neuron, this neuron appears to be a distinct neuron from LNO2. Scale bar is 50 μm .

f. Skeletons of two h Δ B neurons from the hemibrain dataset. Overlaid are the anatomical boundaries of the FB. Spheres denote soma positions.



Extended Data Figure 7: SpsP, LNO2, IbSpsP, and LNO1 physiology.

a. Schematic of SpsP and LNO2 input onto a single PFNd neuron. PFNd neurons have dendrites in the PB on the side ipsilateral to their soma, and dendrites in the NO on the side contralateral to their soma. As a result, PFNd neurons receive input from ipsilateral SpsP neurons and the contralateral LNO2 neuron. Thus, although SpsP and LNO2 neurons have opposite velocity preferences (Fig. 2c), they have congruent effects on PFNd neurons.

b. SpsP and LNO2 activity as a fly walks in closed loop with a visual cue.

c. SpsP and LNO2 $\Delta F/F$ versus lateral velocity in the ipsilateral direction. Data for the right and left PB are combined, binned by the ipsilateral rotational velocity, and averaged across flies (n=8 flies for SPS, 4 flies for LNO2). Because rotational and lateral velocity are correlated, rotational velocity bins are asymmetrically populated. There is a significant effect of lateral velocity (2-way ANCOVA, $P < 10^{-10}$ for both SpsP and LNO2) but not rotational velocity ($p=0.59$ for SpsP, $p=0.14$ for LNO2). Note however that SpsP activity increases when rotational *speed* is high, for both ipsi- and contralateral rotations.

d. Control experiments for SpsP optogenetic activation. There is little effect of light in PFNd recordings from flies where an empty split-Gal4 line is combined with UAS-CsChrimson (n=3) or in flies with UAS-CsChrimson expressed under SpsP split-Gal4 control (ss52267) but reared in the absence of all-trans-retinal (ATR; n=3). We consistently see strong inhibition in flies that express UAS-CsChrimson under SpsP split-Gal4 control (ss52267) and that are raised on culture media containing ATR (n=9, reproduced from Fig. 2d). PFNd recordings were performed in TTX to isolate monosynaptic responses (see Methods).

e. Each IbSpsP neuron receives input from the inferior bridge (IB) and SPS, and projects to a few adjacent PB glomeruli.

f. Circular correlation between visual cue position and IbSpsP bump position (n=8 flies). Shown for comparison is the circular correlation for EPG neurons (n=5 flies), reproduced from Extended Data Fig. 2a.

g. IbSpsP population activity in the PB as a fly walks in closed loop with a visual cue.

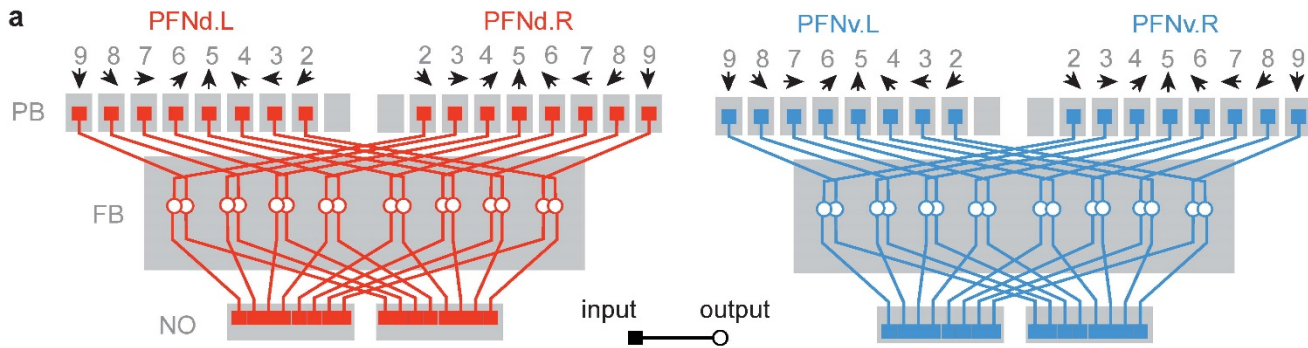
h. Normalized IbSpsP bump amplitude versus forward velocity. Data are binned by lateral velocity in the ipsilateral direction, combined for the right and left PB, and averaged across flies (n=8 flies). There is a significant effect of lateral velocity ($P < 0.01$) but not forward velocity ($p=0.65$, 2-way ANCOVA).

i. Normalized IbSpsP bump amplitude in the PB, versus body-centric translational direction. Data are binned by speed. Lateral velocity is expressed in the direction ipsilateral to the imaged PB, allowing us to combine data from the right and left PB before averaging across flies (n=8 flies).

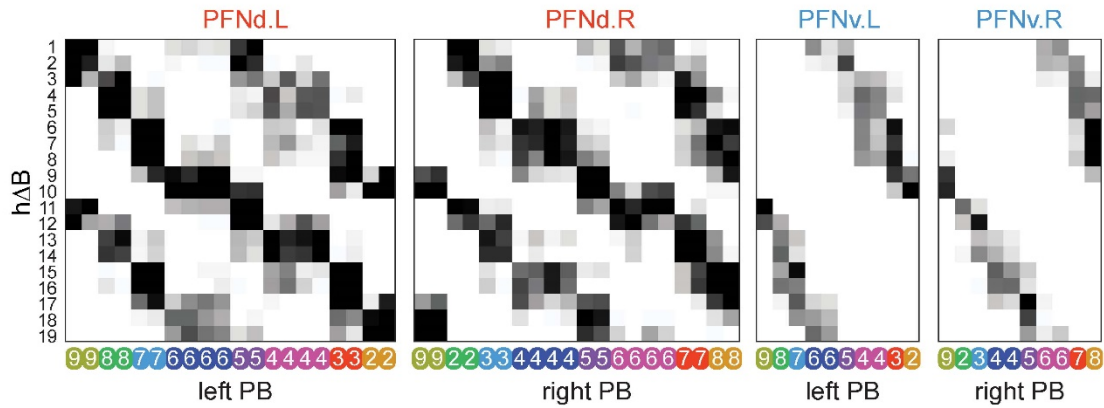
j. Each LNO1 neuron receives input from the LAL and synapses onto PFNv and PFNd dendrites in the NO.

k. LNO1 activity as a fly walks in closed loop with a visual cue. We used jGCaMP7s in these experiments (rather than jGCaMP7f) because LNO1 fluorescence was dim with jGCaMP7f.

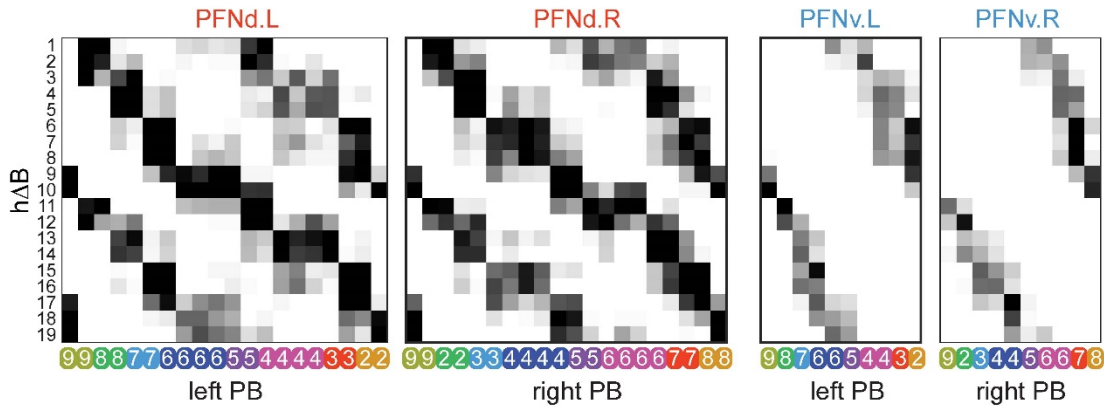
l. LNO1 activity versus forward velocity. Data for the left and right NO are combined, binned by lateral velocity in the ipsilateral direction, and averaged across flies (n=8 flies). LNO1 activity decreases slightly with ipsilateral backward movement. There is a significant effect of both forward velocity ($P < 10^{-10}$) and lateral velocity ($P < 0.01$, 2-way ANCOVAs).



b Actual connectivity



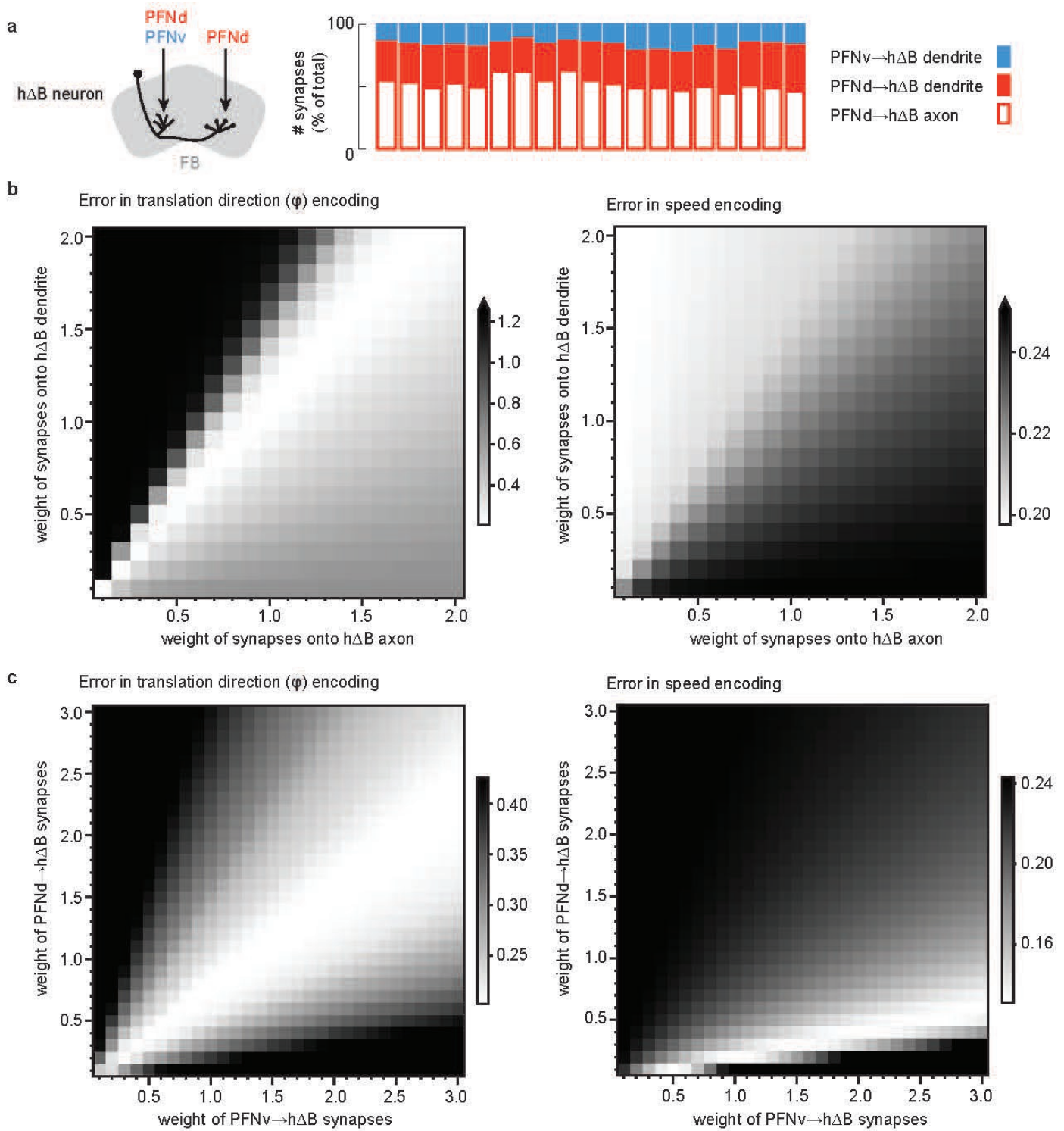
Permuted connectivity (left-right shift eliminated)



Extended Data Figure 8: PFN→hΔB connectivity.

a. Schematized projections of the PFNd and PFNv populations, from the hemibrain connectome. Gray numbers denote PB glomeruli³. Note that the mapping from PB glomeruli to FB horizontal locations is the same for PFNd (red) and PFNv (blue). For each cell type, each half of the PB contains a complete heading map (black arrows) which is projected onto the full horizontal axis of the FB.

b. Top: PFN→hΔB connection matrix from the hemibrain connectome, reproduced from Fig. 3g. Note that, for a given hΔB neuron, PFN projections from the left and right PB are horizontally shifted, corresponding to the morphologies in (a). Bottom: Permuted PFN→hΔB connection matrix. Here, the shifts between left and right PFN matrices are eliminated. We used this permuted connection matrix in Fig. 4d (“left-right shift eliminated”).



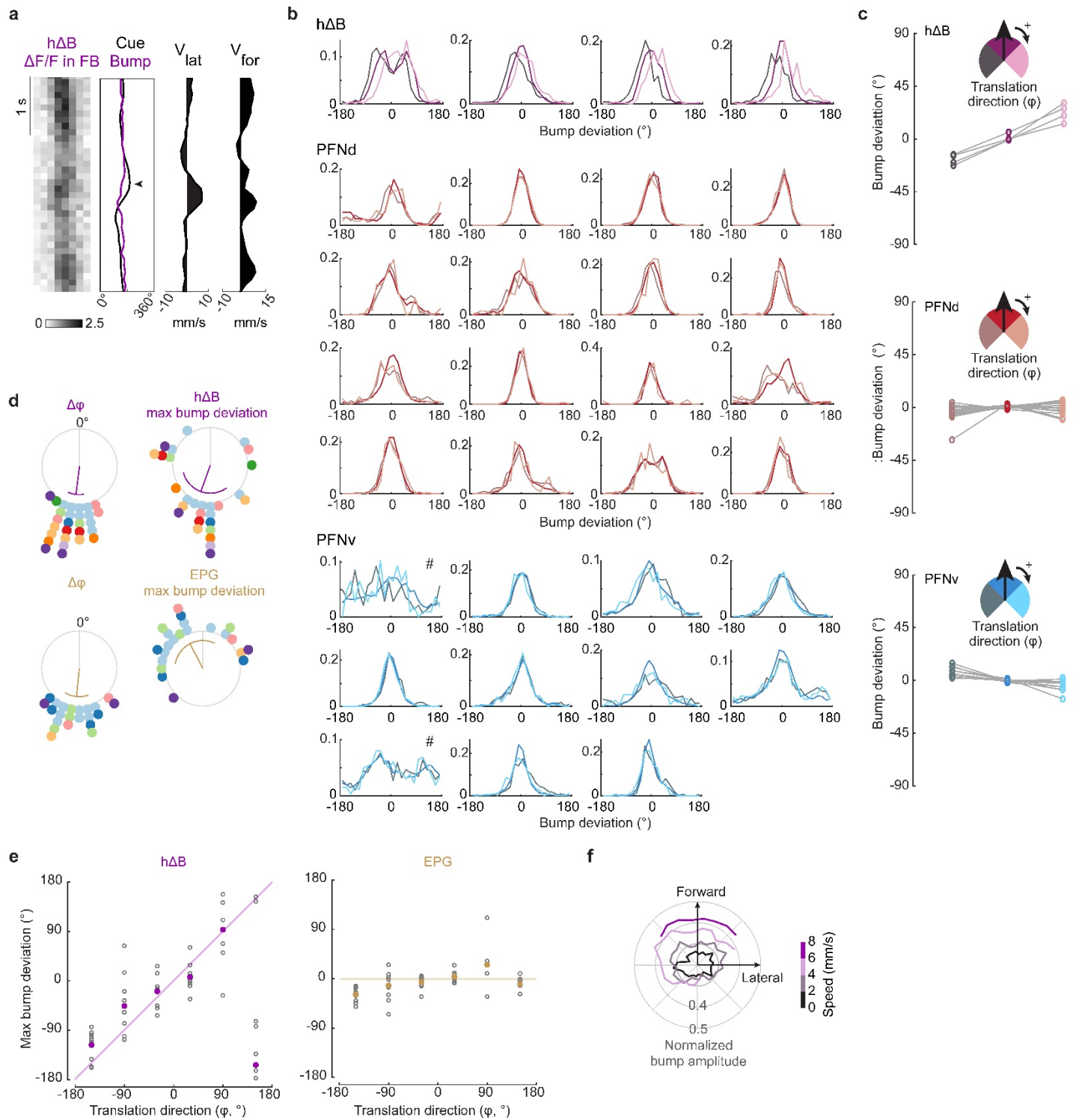
Extended Data Figure 9: Model performance as a function of relative synaptic weight.

a. h Δ B dendrites receive PFNd and PFNv inputs at their dendrites. By contrast, h Δ B axon terminals receive PFNd inputs but no PFNv input. In the bar plot at right, each bar represents one h Δ B neuron in the hemibrain connectome ($n = 19$ neurons). The computational model in Fig. 4a-d assigns an equal weight to all synapses, meaning that all connections are simply weighted by the number of synapses they contain, regardless of whether they are axo-dendritic or axo-axonic connections.

b. To determine if the model might perform better if we treated these connections differently, we systematically varied the weight of PFN synapses onto h Δ B dendrites versus axons, and we used the population vector average of h Δ B activity to

decode the fly's simulated movement. Grayscale heatmap shows the error in translational direction encoding (left) and speed encoding (right), with lower values indicating more accurate encoding. Note that we obtain the best translation direction encoding if we apply equal weight to axo-dendritic or axo-axonic connections (as we do in Fig. 4a-d). Speed encoding improves if we minimize the weight at the synapses onto h Δ B axons; this is because this reduces the contribution of PFNd inputs (relative to PFNv), and so it tends to reduce the disproportionate gain when the fly is walking in the preferred direction φ^p of the PFNd population (Fig. 4c). We do not know whether axo-dendritic and axo-axonic connections are actually weighted equally in the real network, but the fact that we observe good encoding of φ in the h Δ B population (Fig. 4h) suggests that these connections carry similar weight, at least as measured with jGCaMP7f.

c. We also systematically varied the weight of PFNd and PFNv synapses. We obtain the best translation direction encoding if we apply equal weight to PFNd and PFNv connections (as we do in Fig. 4a-d). Speed encoding improves if we reduce PFNd weights, again because this reduces the disproportionate gain when the fly is walking in the preferred direction φ^p of the PFNd population (Fig. 4c).



Extended Data Figure 10: hAB bump deviations

a. hAB $\Delta F/F$ in each FB column as a fly walks in closed loop with a visual cue. When the fly steps laterally (\blacktriangleleft), the bump deviates from the cue.

b. Histograms showing the difference between cue position and bump position, mean-centered in each experiment, and binned by translation direction; $n=4$ flies for hAB, 16 flies for PFNd, and 11 flies for PFNv, # = relatively poor correlation

between cue and bump; these experiments are omitted from panel c. At more lateral translation angles, the h Δ B bump deviates away from where it would be when the fly is walking forward.

c. Mean difference between cue position and bump position. Each set of connected symbols is one experiment. For h Δ B neurons (n=4 flies), we found the shift was significant when comparing left translation-heading deviations to centered translation-heading deviations (P=0.0013, 2-sided paired-sample t-test with Bonferroni-corrected $\alpha = 0.0167$, CI = [-0.460, -0.191] radians) and when comparing right translation-heading deviations to centered translation-heading deviations (P=0.0115, $\alpha = 0.0167$, CI = [-0.698, -0.0473] radians). For PFNd neurons (n=16 flies), the shift is not significant when comparing left translation-heading deviations to centered translation-heading deviations (P=0.0215, 2-sided paired-sample t-test with Bonferroni-corrected $\alpha = 0.0167$, CI = [-0.180, 0.0044] radians) or when comparing right translation-heading deviations to centered translation-heading deviations (P=0.4790, $\alpha = 0.0167$, CI = [-0.0467, 0.0812] radians). For PFNv neurons (n=9 flies; 2 flies were excluded from our analysis), this shift is significant when comparing left translation-heading deviations to centered translation-heading deviations (P=0.0011, 2-sided paired-sample t-test with Bonferroni-corrected $\alpha = 0.0167$, CI = [0.0544, 0.222] radians) but not significant when comparing right translation-heading deviations to centered translation-heading deviations (P=0.0313, $\alpha = 0.0167$, CI = [-0.0135, 0.1848] radians); note that the shift is opposite to h Δ B neurons.

d. Same as Fig. 4f-g but color-coded by fly (n=28 epochs in 10 flies for h Δ B, n=22 epochs in 6 flies for EPG).

e. Maximum bump deviation versus φ , measured in all epochs ≥ 300 ms when the φ was consistent over the epoch. Within each fly, epochs are binned by φ and then averaged (\circ) before averaging across flies (\bullet). For h Δ B neurons, the data are close to the identity line (purple); while for EPG neurons, the data are close to the zero line (gold). n=10 flies for h Δ B, n=10 flies for EPG.

f. Normalized h Δ B bump amplitude versus φ , binned by speed (n=11 flies).